

Mycobacterium tuberculosis induces delayed lipid droplet accumulation in dendritic cells depending on bacterial viability and virulence

Maria Fernanda de Souza Costa ^{1,2,3} | Filipe Pereira-Dutra ⁴ | Nathalie Deboosere³ | Samuel Jouny³ | Ok-Ryul Song³ | Guilherme Iack^{1,4} | Andreia Lamoglia Souza⁵ | Eric Henrique Roma⁵ | Vincent Delorme ³ | Patricia T. Bozza⁴ | Priscille Brodin³

¹Instituto de Biologia, Departamento de Imunobiologia, Universidade Federal Fluminense, Niteroi, Brazil

²Center for Technological Development in Health, Fundação Oswaldo Cruz, Rio de Janeiro, Brazil

³Univ. Lille, CNRS, Inserm, CHU Lille, Institut Pasteur de Lille, U1019 – UMR 9017 - CIL - Center for Infection and Immunity of Lille, Lille, France

⁴Immunopharmacology Laboratory, Instituto Oswaldo Cruz, Fundação Oswaldo Cruz, Rio de Janeiro, Brazil

⁵Fundação Oswaldo Cruz, Laboratory of Immunology and Immunogenetics in Infectious Diseases at Evandro Chagas National Institute of Infectious Diseases, Rio de Janeiro, Brazil

Correspondence

Maria Fernanda de Souza Costa, Instituto de Biologia, Departamento de Imunobiologia, Universidade Federal Fluminense, Niteroi, Brazil.

Email: mf_costa@id.uff.br

Present address

Samuel Jouny, The Institute of Cancer Research, The Breast Cancer Now Toby Robins Research Centre, London, UK

Ok-Ryul Song, The Francis Crick Institute, High Throughput Screening, London, UK

Funding information

Agence Nationale de la Recherche, Grant/Award Number: ANR-10-EQPX-04-01, ANR-16-CE35-0009 and ANR-18-JAM2-0002; European Commission, Grant/Award Number: CycloNHit 608407, ERC-STG INTRACELLTB 260901 and MM4TB 260872; Feder, Grant/Award Number: 12001407 (D-AL) Equipex Imaginex BioMed; Région Nord Pas de Calais, Grant/Award Number: 12000080; European Union; Institut Pasteur, Grant/Award Number: J558, PTR430 and PTR441; Conselho Nacional de Desenvolvimento Científico e Tecnológico, Grant/Award Number: Ciência Sem Fronteiras

Abstract

Tuberculosis remains a global health threat with high morbidity. Dendritic cells (DCs) participate in the acute and chronic inflammatory responses to *Mycobacterium tuberculosis* (Mtb) by directing the adaptive immune response and are present in lung granulomas. In macrophages, the interaction of lipid droplets (LDs) with mycobacteria-containing phagosomes is central to host-pathogen interactions. However, the data available for DCs are still a matter of debate. Here, we reported that bone marrow-derived DCs (BMDCs) were susceptible to Mtb infection and replication at similar rate to macrophages. Unlike macrophages, the analysis of gene expression showed that Mtb infection induced a delayed increase in lipid droplet-related genes and pro-inflammatory response. Hence, LD accumulation has been observed by high-content imaging in late periods. Infection of BMDCs with killed H37Rv demonstrated that LD accumulation depends on Mtb viability. Moreover, infection with the attenuated strains H37Ra and *Mycobacterium bovis*-BCG induced only an early transient increase in LDs, whereas virulent Mtb also induced delayed LD accumulation. In addition, infection with the BCG strain with the reintroduced virulence RD1 locus induced higher LD accumulation and bacterial replication when compared to parental BCG. Collectively, our data suggest that delayed LD accumulation in DCs is dependent on mycobacterial viability and virulence.

KEYWORDS

dendritic cell, immunometabolism, lipid droplets, RD1, tuberculosis

1 | INTRODUCTION

Tuberculosis is an airborne disease caused by *Mycobacterium tuberculosis* (Mtb) that presents high morbidity rates. It is estimated that one-third of the world's population is latently infected with Mtb and that 10 million people developed the disease in 2021, resulting in more than 1.6 million deaths (World Health Organization, 2022). The host immune response is usually sufficient to contain the infection but may not fully eradicate dormant bacteria (Kilinç et al., 2021). There is only one vaccine named Bacillus Calmette-Guérin (BCG), an attenuated strain of *Mycobacterium bovis* widely used worldwide. However, studies suggest that although BCG has effect on limiting disease dissemination in children, it fails to prevent adult pulmonary infection. The current therapy for tuberculosis requires long treatment with multiple antibiotics, which presents several side effects. This treatment has reduced effects on dormant bacilli and increased risks of failure due to emerging drug resistance (Dartois & Rubin, 2022). Therefore, elucidating the molecular mechanisms involved in the immune response to mycobacterial infection could provide important insights into further developing new therapies and vaccines.

DCs play a crucial role in initiating and determining the type of immune response produced against the pathogen through the secretion of cytokines and expression of costimulatory molecules (Tian et al., 2005; Tzelepis et al., 2015; Zhang et al., 2013). During virulent Mtb infection, DCs present reduced antigenic presentation capacity and a tolerogenic phenotype, which limits T-cell proliferation and Th1 differentiation (Kim et al., 2016; Morris et al., 2013; Rodrigues et al., 2020; Wolf et al., 2007). Interestingly, Tailleux and coworkers (2003) showed that Mtb presented a lower replication rate in human dendritic cells than in macrophages through a bacteriostasis mechanism.

DCs participate in the acute and chronic inflammatory response to Mtb and are present in both mouse and human lung granulomas (Schreiber et al., 2011; Uehira et al., 2002). Published data demonstrate that some of the foamy cells in Mtb-induced mouse granulomas and lung biopsies of tuberculosis patients express DC markers (Hunter et al., 2011; Ordway et al., 2005). The foamy phenotype occurs through the accumulation of lipid droplets (LDs), which are neutral lipid-rich, specialized organelles that play a wide range of roles in cell signaling and activation, regulation of lipid metabolism, membrane trafficking, and control of the synthesis and secretion of inflammatory and anti-inflammatory mediators (Pereira-Dutra et al., 2019). LD accumulation is correlated with granuloma formation and seems to be the prerequisite for the transition of Mtb from active replication to dormancy (Kapoor et al., 2013; Mattos et al., 2011; Santucci et al., 2016).

Mtb-infected macrophages present an increase in size and in the number of LDs (Brandenburg et al., 2021; Caire-Brändli et al., 2014;

Knight et al., 2018; Laval et al., 2021; Neyrolles, 2014). Host lipids are shown to serve as a carbon source for Mtb and other mycobacterial species during infection. Reports in the *M. marinum*-infected *Dictyostelium discoideum* model demonstrate that host LDs are directed to *Mycobacterium*-containing vacuoles, where lipids are captured by the bacteria (Barisch et al., 2015). LD-phagosome interactions are controlled by mycobacterial cell wall components and host Rab7, which enables the exchange of contents between LDs and phagosomes (Roque et al., 2020). Indeed, Mtb is found close to LDs, and the utilization of fatty acids by Mtb was shown to facilitate Mtb intracellular survival and persistence in vivo (Brandenburg et al., 2021; Muñoz-Eliás & McKinney, 2005; Pandey & Sasseti, 2008; Peyron et al., 2008). On the other hand, host factors induce LD formation in mycobacterial-infected macrophages, contributing to host immune defense by supporting the production of eicosanoids, in addition to bacterial factors (D'Avila et al., 2006; Knight et al., 2018; Mattos et al., 2011).

Despite studies on the mechanisms of LD formation during mycobacterial infection in macrophages, there are few studies in the literature describing this phenomenon in DCs using other disease models (Gao et al., 2015; Herber et al., 2010; Lecoeur et al., 2013; Meester et al., 2014). The role of LDs in DC biology is still unclear and contradictory in the literature. It has been shown in DCs that LPS-induced LD accumulation is required for phagosome maturation and cross-presentation of antigens via MHC class I (Bougnères et al., 2009). Conversely, a reduced capacity in the processing and presentation of antigens by lipid-rich DCs was demonstrated (Gao et al., 2015; Herber et al., 2010). Thus, it is important to determine whether this process occurs differently in DCs than in macrophages, providing a better knowledge of DC and Mtb interactions. Herein, we demonstrate that LD accumulation in DCs during Mtb infection occurs at a later time point than in macrophages and that this phenomenon depends on bacterial viability and virulence.

2 | RESULTS

2.1 | Mtb replicates in BMDCs

Primarily, we assessed the susceptibility of mouse bone marrow-derived DCs (BMDCs) to Mtb infection. Therefore, we performed a cellular fluorescence-based high-content assay previously developed by our group (Christophe et al., 2009; Song et al., 2017). Using this pipeline, we were able to detect different cell populations, such as dendritic cells, bacteria, and infected cells, by quantitative analysis of confocal microscopy images (Figures S1 and S2). Automated confocal microscopy allowed us to track the increase in the intracellular bacterial area per cell through analysis of the same field of view in kinetics (Figure 1a). Then, we evaluated

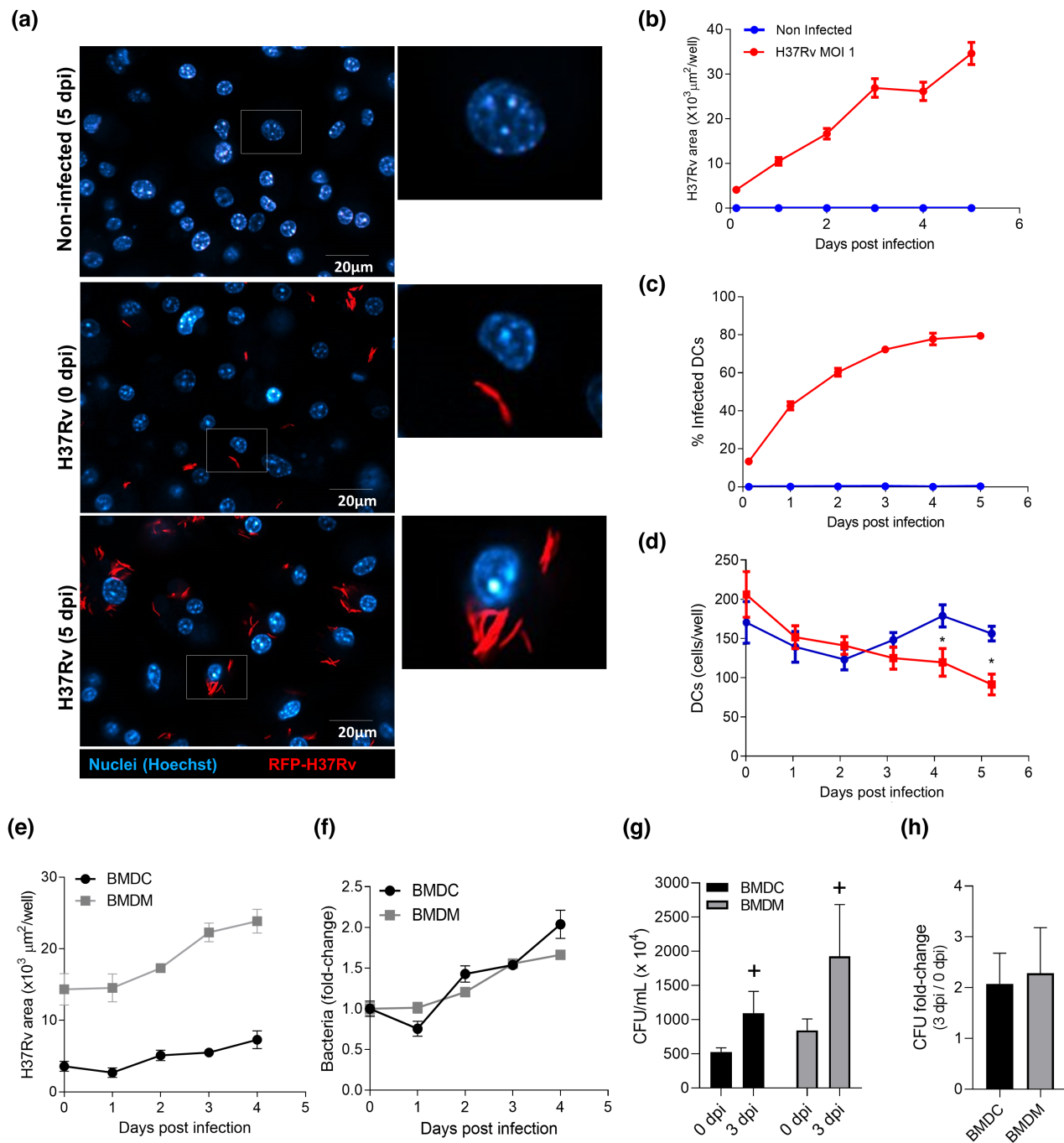


FIGURE 1 Mtb replicates in mouse BMDCs. BMDCs were infected with Mtb RFP-H37Rv (MOI of 1) for 2 h. (a) Representative pictures (63X) of H37Rv (red) growth in BMDCs stained with Hoechst (blue) at 0 and 5 days postinfection obtained by confocal fluorescence microscopy. (b) Kinetics of Mtb growth measured by H37Rv area per well, (c) percentage of infected, and (d) the number of dendritic cells/well. (e) BMDCs, bone marrow-derived macrophages (BMDMs), and cells were infected with Mtb H37Rv (MOI of 1) for 2 h. Kinetics of Mtb growth measured by (f) bacterial area/well and multiplication factor of total bacterial area (g) from day 0 postinfection. Data were obtained by quantitative analysis of confocal fluorescence microscopy images and are represented as the average \pm SEM for at least five replicated wells. Intracellular bacterial CFU enumeration in BMDCs and BMDMs infected with H37Rv at 0 dpi and 3 dpi (h). Intracellular bacterial CFU fold change (3 dpi/0 dpi) within BMDCs and BMDMs (j). Data from one representative experiment are represented as the average \pm SEM for at least four replicates. *Indicates statistically significant differences ($p \leq 0.05$) between nonstimulated and infected groups; + indicates statistically significant differences ($p \leq 0.05$) between 0 dpi and 3 dpi, as determined by Student's *t*-test

the growth kinetics of Mtb H37Rv expressing RFP in mouse bone marrow-derived DCs (BMDCs). We observed the growth of Mtb in mouse BMDCs, as illustrated by the increase in the H37Rv area

and the increase in the percentage of infected cells from 1 to 5 days postinfection (dpi) (Figure 1b,c). Moreover, H37Rv infection significantly reduced the number of cells per well (approximately

30–40%) from 4 dpi to 5 dpi compared to the noninfected group (Figure 1d). In addition, we compared H37Rv replication kinetics between BMDCs and well-described bone marrow-derived macrophages (BMDMs). We observed that at all time points, the total area of intracellular bacteria in infected cells was higher in BMDMs than in BMDCs (Figure 1e). Indeed, BMDMs presented increased bacterial area and colony-forming units (CFU) 3 h postinfection (hpi) compared to BMDCs (Figure S3). However, the rate of increase in the bacterial area from 0 to day 4 dpi was similar in both cell types (Figure 1f). To validate these results, bacterial viability was assessed by CFU enumeration. We observed an increase in H37Rv-CFU enumeration from 0 dpi to 3 dpi for both BMDCs and BMDMs (Figure 1g), with a similar fold increase (Figure 1h). These results reinforce that Mtb replicates inside BMDCs at a similar rate to BMDMs.

2.2 | Mtb infection induced delayed immunometabolic reprogramming in BMDCs

To better understand the BMDC response to Mtb infection, we analyzed the expression of pro- and anti-inflammatory genes. We observed that H37Rv infection induced a proinflammatory response in BMDCs on the first day of infection (1 dpi), characterized by an increase in inducible nitric oxide synthase (*inos/nox2*), cyclooxygenase-2 (*cox-2/ptgs2*), and major histocompatibility complex class I-related (*mr1*) gene expression (Figure 2a). Despite the increase in interleukin-10 (*il-10*) expression in Mtb-infected BMDCs at 3 dpi, we observed a predominant proinflammatory response characterized by the upregulation of interleukin-1 β (*il-1\beta*), *inos*, *cox-2*, 5-lipoxygenase (*5-lo*), and *mr1* genes at 3 dpi (Figure 2b) and the downregulation of the anti-inflammatory macrophage marker chitinase-3-like protein 3 (*chi3l3/ym1*).

Therefore, we compared the BMDC and BMDM responses to Mtb infection. In BMDMs, H37Rv infection induced an early mixed response in which both proinflammatory (*il-1\beta*, *inos*) and anti-inflammatory (*il-10*, Arginase-1 - *arg-1*) genes were upregulated (Figure 2c). In addition, we observed that Mtb infection in BMDMs induced an increase in *cox-2* expression and downregulation of *5-lo* expression at 1 dpi (Figure 2c). This mixed inflammatory response seems to induce a late M2-related response, exemplified by the upregulation of *chi3l3*, *arg-1*, *il-10*, and *cox-2* in H37Rv-infected BMDMs (Figure 2d).

Metabolic reprogramming is critical for dendritic cell and macrophage immune function (O'Neill & Pearce, 2016). Our next step was to compare how lipid metabolism is modulated by Mtb infection in BMDCs and BMDMs. We observed that Mtb triggered the overexpression of the main genes associated with neutral lipid metabolism and lipid droplet formation in both BMDMs and BMDCs (Figure 2e–h). However, the time course of this modulation was temporally different between BMDCs and BMDMs. In BMDCs, we observed

that H37Rv infection induced a delayed upregulation of *fatty acid synthase (fasn)*, *enzymes of neutral lipid synthesis (dgat1, dgat2, and acat1)*, LD-structural proteins (*plin2* and *plin3*), and the major triglyceride lipase (*atgl*) genes (Figure 2f). Notably, Mtb infection did not affect the expression of the analyzed genes at 1 dpi (Figure 2e). In contrast, Mtb-infected BMDMs presented an early change in the expression of enzymes of neutral lipid synthesis (*dgat1* and *acat1*), lipid uptake (*cd36*), one of the main LD-structural proteins perilipins (*plin2*), and lipase ATGL (*atgl*) (Figure 2g). At 3 dpi, we observed that only perilipins (*plin 2* and *plin 3*) mRNA remained increased and that *dgat1* and *acat1* genes were repressed in infected macrophages (Figure 2h).

2.3 | Mtb induces lipid droplet accumulation in BMDCs

We next evaluated whether Mtb infection could induce lipid droplet accumulation in BMDCs. We assessed LD accumulation using the neutral lipid probe LipidTOX™ Deep Red neutral lipid and quantified it by fluorescence-based high-content analysis. At 4 dpi, we observed an increase in LD accumulation in BMDCs (Figure 3a), determined by the increase in LD number per cell (Figure 3b), LD area per cell (Figure 3c), and LipidTOX fluorescence intensity (Figure 3d) when compared to the unstimulated control. The level of LD accumulation induced by Mtb infection in BMDCs was similar to that induced by lipopolysaccharide (LPS), a well-known inducer of LD accumulation in leukocytes (Figure 3a–d). To support these results, we extracted lipids from BMDCs, and we observed that Mtb induced mainly the accumulation of cholesterol ester (CE) with a low presence of triglycerides by thin-layer chromatography (TLC) at 3 dpi (Figures 3e and S4).

Then, we evaluated whether the presence of bacteria in BMDCs could influence the number of LDs per cell. Interestingly, the number of LDs per cell was significantly higher in BMDCs containing H37Rv than in bystander cells that did not contain bacteria (Figure 3f). Nevertheless, noninfected cells presented an increase in LD accumulation, probably due to host mediators present in the supernatant, suggesting that LD accumulation in BMDCs during Mtb infection may not be restricted to direct cell interaction with Mtb. We also observed the proximity between Mtb and LDs, which suggested an interaction between them in BMDCs (Figure 3g) that should be further confirmed. To determine whether bacterial viability was required for LD accumulation, we infected DCs with formalin-killed (FK)-H37Rv. We observed that FK-H37Rv induced a slight increase in LD accumulation in BMDCs (Figure 3h), suggesting that bacterial interaction and internalization could be sufficient to induce LD accumulation. However, the stimulation remained below that observed with live H37Rv, indicating that bacterial replication (Figure 3i) is central to LD accumulation.

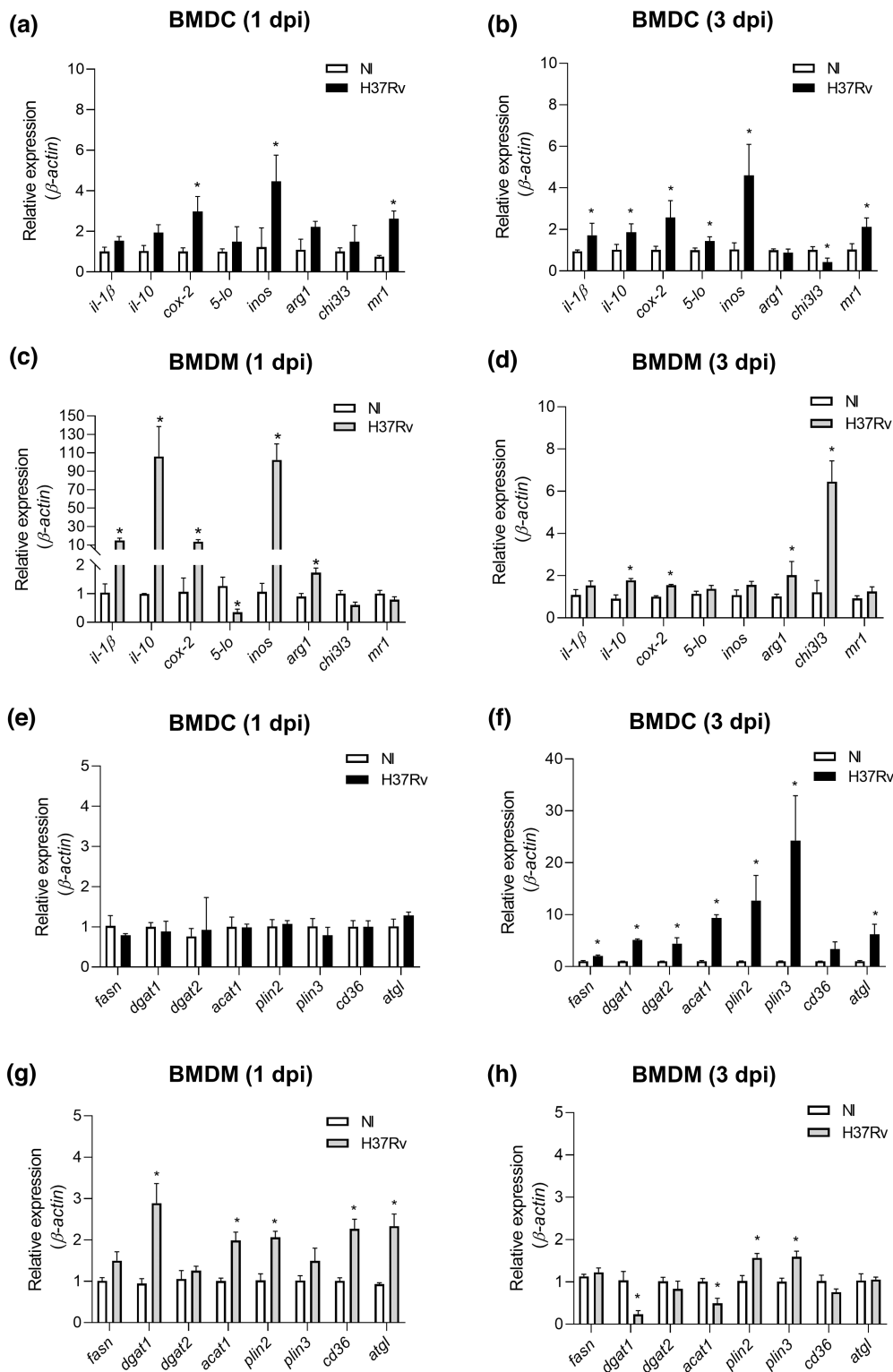


FIGURE 2 Mtb infection induces delayed immunometabolic reprogramming in mouse BMDCs. BMDCs were infected with Mtb H37Rv (MOI of 1) for 2 h. (a–d) relative mRNA expression of immune response genes (*il-1β*, *il-10*, *cox-2*, *5-lo*, *inos*, *arg1*, *chi3l3*, *mr1*) from BMDCs at 1 dpi (a) or 3 dpi (b) and BMDMs at 1 dpi (c) or 3 dpi (d) measured by qPCR analysis. (e–h) Relative mRNA expression of lipid metabolism-related genes (*fasn*, *dgat1*, *dgat2*, *acat1*, *plin2*, *plin3*, *atgl*, and *cd36*) in BMDCs at 1 dpi (e) or 3 dpi (f) and BMDMs at 1 dpi (g) or 3 dpi (h) measured by qPCR analysis. Bars are the mean $2^{-\Delta\Delta Ct} \pm SEM$; $n = 6$; * $p < 0.05$, Student's *t*-test compared to control. Data from one representative experiment are represented as the average $\pm SEM$ for at least four replicates

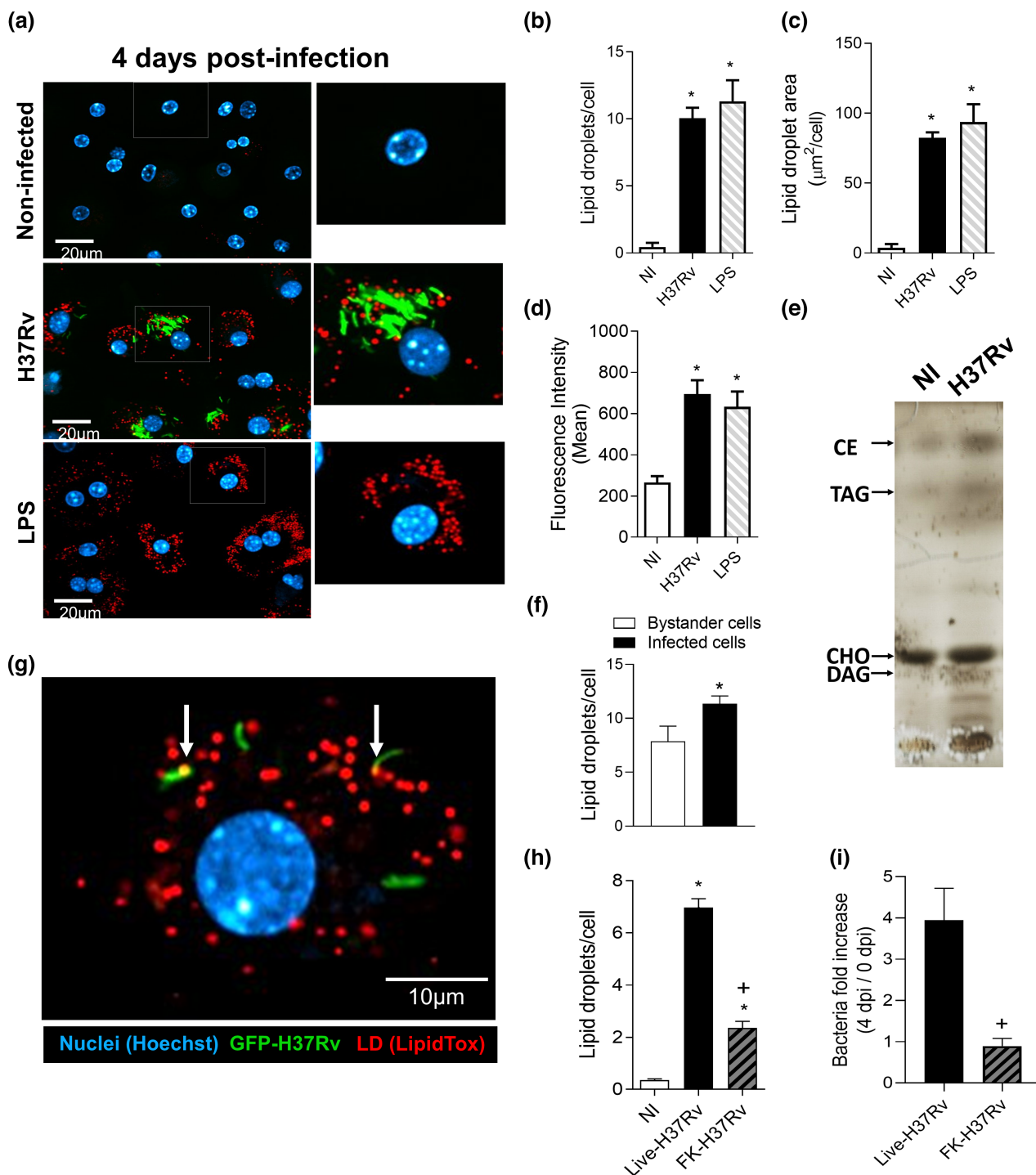


FIGURE 3 Mtb infection induces LD accumulation in mouse BMDCs. Cells were infected with GFP-H37Rv at an MOI of 1:1 or treated with LPS (10 ng/ml). At day 4 dpi, fixed BMDCs were stained with neutral lipids HCS LipidTOX dye. (a) Representative images (63X) of LD (red) accumulation induced by H37Rv (green) infection or LPS stimulation (10 ng/ml) in BMDCs stained with Hoechst (blue). (b–d) LD accumulation in BMDCs was evaluated by (b) LD number per cell, (c) LD area per cell, and (d) mean fluorescence intensity (MFI) per cell. (e) Representative thin layer chromatography (TLC) of neutral lipids from DCs at 3 dpi. Standards: Cholesterol ester (CE), cholesterol (C), triacylglycerol (TG), and diacylglycerol (DG). (f) Differential analysis of LD number in infected and bystander cells within 4 dpi. (g) Representative image of LD and H37Rv interaction (arrows) in infected BMDCs. Comparison of (h) LD accumulation and (i) bacterial replication in BMDCs infected with H37Rv and formalin-killed (FK) bacteria. Data were obtained by quantitative analysis of confocal fluorescence microscopy images and are represented as the average \pm SEM for at least five replicated wells from one representative experiment. *Indicates statistically significant differences ($p \leq 0.05$) between nonstimulated and stimulated groups; + indicates statistically significant differences ($p \leq 0.05$) between live H37Rv- and FK-killed H37Rv-infected groups, as determined by Student's *t*-test

2.4 | Delayed lipid droplet accumulation in infected BMDCs depends on Mtb virulence genes

Since our results indicated that Mtb-triggered LD accumulation in BMDCs is strongly dependent on bacterial viability, we further evaluated whether this process is related to Mtb virulence by infecting cells with H37Ra and *M. bovis* BCG (Figure 4a–d). Interestingly, we observed early and transient LD accumulation 3h after mycobacterial infection, which returned close to baseline levels at 1 dpi and was not related to virulence factors. At 1 dpi, H37Rv-infected BMDCs presented the same LD numbers (Figure 4a) and LD area (Figure 4b) as BMDCs infected with H37Ra and BCG. Moreover, all three groups presented the same bacterial area at this time point (Figure 4d). Nevertheless, at late time points, H37Rv induced LD accumulation starting at 2 dpi, reaching higher levels at 3 dpi that were not observed in DCs infected with attenuated strains (Figure 4a,b), suggesting a correlation of LD induction with strain virulence. Notably, the H37Ra and BCG bacterial areas did not increase, whereas virulent Mtb replicated in BMDCs (Figure 4c,d). The inability of BCG to replicate inside BMDCs was also observed through CFU fold change analysis (Figure 4e).

The principal genetic basis for BCG attenuation is the loss of the region of difference 1 (RD1), which encodes several components of the ESX-1 type IV secretion system (Majlessi et al., 2005; Pym et al., 2002; Simeone et al., 2015). On the other hand, H37Ra presents a similar genome structure to virulent H37Rv with few single nucleotide polymorphisms (SNPs) essential for bacterial virulence, including the ESX-1 secretion-associated protein (EspK) gene (Jia et al., 2017). Then, to assess the role of mycobacterial virulence factors in LD accumulation in BMDCs, we evaluated the effect of RD1 region reintroduction in BCG (BCG::RD1) (Figure 4f–i). We observed that BCG::RD1 induced a higher LD area per cell after 4 dpi (Figure 4f,i), mainly on infected cells (Figure 4g), and that this bacteria could replicate inside BMDCs (Figure 4h) when compared to BCG-infected cells. Taken together, these results reinforced that mycobacterial viability and replication are strongly associated with LD accumulation in DCs.

3 | DISCUSSION

In the present work, we evaluated LD accumulation and lipid metabolism reprogramming in BMDCs during Mtb infection. Metabolic reprogramming is related to immune cell functions, including cytokine production, phagocytosis, and antigen presentation (O'Neill & Pearce, 2016). LDs are associated with bacterial survival and host-cell immune response (Brandenburg et al., 2021; Caire-Brändli et al., 2014; Knight et al., 2018; Laval et al., 2021; Neyrolles, 2014). Although many data demonstrate LD accumulation in macrophages (Almeida et al., 2009; Brandenburg et al., 2021; Daniel et al., 2011; D'Avila et al., 2006; Knight et al., 2018; Laval et al., 2021; Mahajan et al., 2012; Peyron et al., 2008; Singh et al., 2012), very few data concerning their accumulation in DCs during mycobacterial infection are available (Machelart et al., 2022).

Herein, we report that Mtb infection induced delayed metabolic reprogramming by inducing fatty acid synthesis and LD accumulation in BMDCs depending on mycobacterial viability and virulence factors. Recent studies have shown that lipid metabolism is a suitable target for host-directed adjunctive treatment of pulmonary TB (Bosch et al., 2020; Brandenburg et al., 2021). Therefore, our findings may provide new insights for developing new host-directed therapies and vaccines.

The ability of Mtb to proliferate inside DCs is still controversial in different in vitro models based on CFU counts. Herein, we followed bacterial growth in DCs by quantitative analysis of confocal fluorescence microscopy images and CFU. Our results confirmed that Mtb could replicate in murine BMDCs to the same extent as in macrophages. Accordingly, in vitro studies have demonstrated the uptake and growth of mycobacteria in human and murine DCs (Buettner et al., 2005; Förtsch et al., 2000; Olakanmi et al., 2013; Rivero-Lezcano et al., 2010). On the other hand, Tailleur and coworkers (2003) described reduced Mtb replication in human monocyte-derived DCs in the presence of IL-4 and GM-CSF. In addition, it has been shown that the total intracellular Mtb loads in human infected-DCs were compatible with limited bacterial growth. However, when these numbers were normalized to the number of live DCs, the number of bacteria per cell increased due to a massive reduction in cell number in the first 3 days of infection (Mendum et al., 2015).

LD accumulation has been demonstrated in murine DCs infected with *Leishmania amazonensis* or *Nocardia brasiliensis* or taken from cancer mouse models (Gao et al., 2015; Herber et al., 2010; Lecoœur et al., 2013; Meester et al., 2014). Changes in metabolism may define the phenotype of immune cells. DC activation preferentially induces a metabolic shift to glycolysis and de novo synthesis of fatty acids, which are involved in cytokine production. Moreover, DCs with high lipid content are associated with immunogenic cells, while cells with lower lipid concentrations seem to be more tolerogenic (Kelly & O'Neill, 2015). Consistent with this, we showed that mycobacterial infection also induced LDs and the upregulation of fatty acid enzymes in parallel with a major proinflammatory phenotype in BMDCs. Fatty acids, triglycerides, and cholesterol stored by host cells are vital sources of energy for mycobacteria and are important during latent-phase infection (Brandenburg et al., 2021; Brzostek et al., 2009; Dawa et al., 2021; Pandey & Sasseti, 2008; Peyron et al., 2008). We observed that Mtb infection increased the expression of the triglyceride synthesis enzymes *dgat1* and *dgat2*, and *acat1*, which are responsible for cholesterol ester formation; however, infected DCs mainly accumulated cholesterol esters at 3 dpi.

Furthermore, we observed that DC infection with virulent (H37Rv) and attenuated strains (H37Ra or *M. bovis*-BCG) induced an early transient increase in LDs per cell. In contrast, virulent H37Rv also induced delayed LD accumulation. Accordingly, H37Ra induces lower LD accumulation than H37Rv in macrophages, a phenomenon dependent on ESAT-6 secretion (Mahajan et al., 2012; Singh et al., 2012). Moreover, *Mycobacterium smegmatis*, another avirulent strain, is not able to induce LD accumulation in these cells (Almeida et al., 2009; Daniel et al., 2011). In agreement, virulent mycobacteria

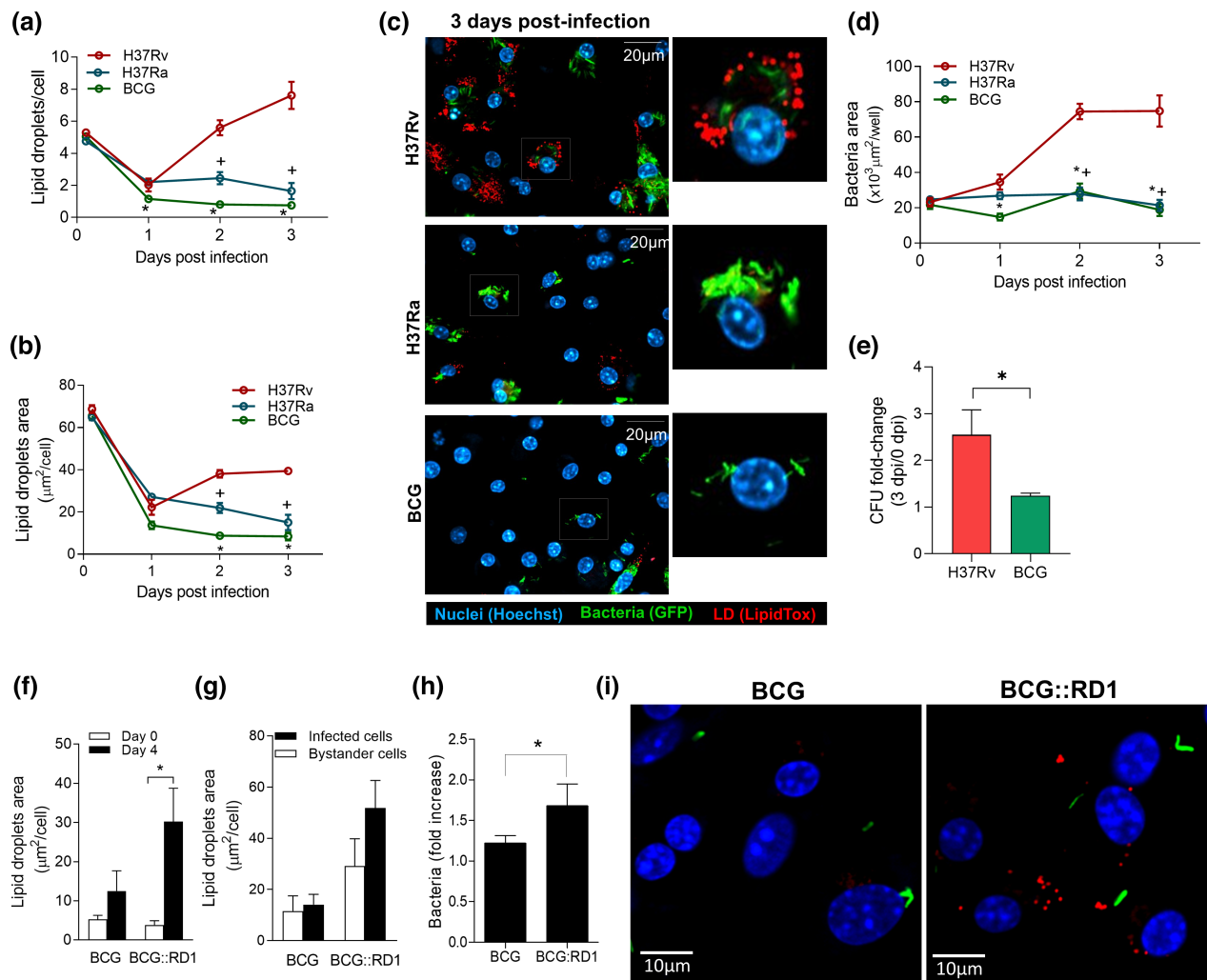


FIGURE 4 LD accumulation in mouse BMDCs during mycobacterial infection is dependent on virulence. Cells were infected with Mtb GFP-H37Rv, Mtb GFP-H37Ra GFP, *Mycobacterium bovis*-BCG GFP, or *M. bovis* BCG::RD1 GFP at an MOI of 1. At the indicated time points, cells were fixed and stained with Hoechst and neutral lipids HCS LipidTOX dye. Kinetics of LD accumulation by (a) number and (b) area after infection with the different mycobacterial strains. (c) Representative images (63X) of LD (red) accumulation induced by H37Rv, H37Ra, or BCG (green) infection in BMDCs stained with Hoechst (blue) at 3 dpi. (d) Kinetics of bacterial growth after infection with the different mycobacterial strains. *Indicates statistically significant differences ($p \leq 0.05$) between H37Rv-infected and BCG-infected groups; +indicates statistically significant differences ($p \leq 0.05$) between H37Rv-infected and H37Ra-infected groups, as determined by Student's *t*-test. (e) Intracellular bacterial CFU fold change (3 dpi/0 dpi) within Mtb- or BCG-infected BMDCs. (f–i) cells were infected with *M. bovis*-BCG GFP or *M. bovis*-BCG::RD1 GFP at an MOI of 1:1. (f) LD area per cell analysis at days 0 and 4 postinfection and (g) comparison between noninfected and infected cells at day 4. (h) Representative images (63X) of LD (red) accumulation induced by BCG or BCG::RD1 (green) infection in BMDCs stained with Hoechst (blue) at 3 dpi. (i) Bacterial growth was determined by the fold increase in the bacterial area from day 0 to 4. Data were obtained by quantitative analysis of confocal fluorescence microscopy images and are represented as the average \pm SEM for at least five replicated wells from one representative experiment. *Indicates statistically significant differences ($p \leq 0.05$), as determined by Student's *t*-test or ANOVA

interact with host LDs and incorporate their lipids as a carbon source, facilitating intracellular survival (Barisch & Soldati, 2017; Brandenburg et al., 2021).

On the other hand, Knight et al. (2018) demonstrated that mycobacteria-induced LD accumulation in BMDMs was not driven by bacterial virulence factors, suggesting that it is a process dependent on the activation of the host immune defense. Recently, IL-17 was discovered to induce LD accumulation in DCs by stimulating the capture of extracellular lipids (Salvatore et al., 2015). In

fact, we observed in our model that DCs that do not contain Mtb presented an increased number of LDs, which was lower than that of H37Rv⁺ DCs, suggesting that both bacterial and host immune factors may induce lipid accumulation in DCs. Indeed, the regulation of LDs through mycobacterial cell wall components by LD association with phagosomes containing beads coated with Mtb lipids, LAM and PIM, has been demonstrated in macrophages (Roque et al., 2020). Whether LD accumulation represents a benefit or disadvantage to the host immune response remains to be investigated. FK-H37Rv

induced only mild LD accumulation, suggesting that other factors, such as active protein secretion or bacterial replication, are important for LD accumulation. Nevertheless, the participation of host immune factors in LD accumulation cannot be excluded and will need to be investigated further. In addition, BMDCs containing bacteria presented higher LD numbers, which interact with the bacilli. Thus, the late accumulation of these organelles may provide nutrients for Mtb. However, further studies are needed to confirm the participation of LDs in bacterial fitness within host cells.

The active secretion of bacterial virulence factors may also be involved in LD induction in DCs, as we showed that bacterial viability is important for LD accumulation. Furthermore, our results demonstrate the contribution of virulence factors to LD accumulation in BMDCs. Compared to virulent H37Rv, H37Ra presents few SNPs, including the EspK gene (Jia et al., 2017). BCG's most important deleted region is RD1, which encodes the (Majlessi et al., 2005; Pym et al., 2002; Simeone et al., 2015). Both attenuated strains H37Ra and *M. bovis*-BCG lack the expression of ESX-1-secreted virulence factors, including CFP-10 and ESAT-6 (Mostowy et al., 2004). RD1 gene products are related to an increase in Mtb virulence and fitness inside DCs and the biosynthesis of lipids from the bacterial cell wall (Mendum et al., 2015). Furthermore, RD1-encoded virulence proteins are also related to DC activation, inducing a tolerogenic phenotype in mycobacteria-infected DCs (Etna et al., 2015; Kim et al., 2016). Accordingly, the reintroduction of the RD1 locus in the BCG strain increased LD accumulation and bacterial replication.

Mtb survives and proliferates in host cells by inhibiting phagosomal acidification, altering cell metabolism, and manipulating cell signaling and antigen presentation (Srivastava et al., 2014). Among the cell populations infected in vivo, myeloid DCs are predominant in the lungs and lymph nodes at later time points. Those infected DCs are poorly effective in stimulating Th1 responses while showing sustained surface expression of MHC-II (Wolf et al., 2007). In vitro studies also show that virulent Mtb infection reduces the DC capacity of antigen presentation by inducing a tolerogenic phenotype that limits T-cell proliferation and Th1 differentiation (Kim et al., 2016; Morris et al., 2013; Rodrigues et al., 2020). During Mtb infection, MHC-I and MHC-II molecules are retained on phagosomes containing live bacteria (Clemens & Horwitz, 1995). The role of LDs in DC biology is still unclear and contradictory in the literature. It has been shown in DCs that LDs are necessary for phagosome maturation and cross-presentation of antigens via MHC class I (Bougnères et al., 2009). Conversely, lipid-rich DCs present dysfunctions in antigen presentation, such as the lower expression of costimulatory molecules and cytokines, and cannot induce CD4 T lymphocyte proliferation (Gao et al., 2015; Herber et al., 2010). Therefore, LD accumulation in DCs during Mtb infection may be correlated with antigen presentation and activation of the adaptive immune response; however, studies are still needed to prove this phenomenon's beneficial or deleterious effects on host immunity.

The cellular response of DCs to Mtb is an underexplored subject, and most studies have only evaluated T cell responses (Rodrigues et al., 2020). In conclusion, we demonstrate that Mtb replicates

inside BMDCs, inducing LD accumulation, which is correlated with strain virulence and bacterial replication. Further studies are required to elucidate the role of LD accumulation and lipid metabolism during tuberculosis and the molecular pathways controlling this phenomenon in DCs.

4 | EXPERIMENTAL PROCEDURES

4.1 | Animals

Six- to eight-week-old female C57BL/6 mice were purchased from Janvier (France) and bred at the Institut Pasteur de Lille experimental animal facility. All mice were maintained and bred in the animal facility of the Pasteur Institute of Lille, France (agreement C59-350009). All experimental procedures received ethical approval from the French Committee on Animal Experimentation and the Ministry of Education and Research (APAFIS#10232-2017061411305485 v6, approved on September 14, 2018).

4.2 | Dendritic cell and macrophage differentiation

Murine bone marrow-derived dendritic cells (BMDCs) or macrophages (BMDMs) were generated from tibia and femur hematopoietic precursors of C57BL/6 mice. BMDCs were differentiated in the presence of GM-CSF as previously described (Lecoeur et al., 2013). Tibia and femurs of C57BL/6 mice were recovered and flushed to obtain the bone marrow. Cells were seeded at a density of 4×10^6 cells per cell culture-treated petri dish (90 mm diameter) in 10 ml of Iscove's modified Dulbecco's medium (IMDM, Lonza) supplemented with 10% heat-inactivated fetal bovine serum (FBS; Invitrogen), 1.5% supernatant from the GM-CSF-producing J558 cell line (kindly provided by Dr. Trottein) and 50 μ M 2-mercaptoethanol. Cultures were incubated at 37°C with 5% CO₂. Fresh medium was added every 3–4 days. On day 10, loosely adherent cells were harvested using DPBS containing 2 mM EDTA. The percentages of CD11c⁺ positive cells ($\approx 90\%$) were determined by flow cytometry (Figure S5; FACSFortessa, BD Bioscience). BMDMs were obtained by seeding 1×10^7 bone marrow cells in 20 ml of RPMI1640 GlutaMAX (Gibco) medium supplemented with 10% FBS and 10% L929-derived M-CSF conditioned medium per 75 cm²-tissue culture flasks (Deboosere et al., 2021). Cells were incubated at 37°C with 5% CO₂ for 6 days. The fresh medium was replaced after 3 days.

4.3 | Mycobacterial strains and growth conditions

Mtb H37Rv, H37Ra, *M. bovis* BCG, and *M. bovis* BCG::RD1 (previously described by Pym et al., 2002) expressing RFP or GFP used in the present study were from stocks held at the Institut Pasteur de Lille, France. Mtb H37Rv, H37Ra, and *M. bovis* BCG::RD1 were

cultured at 37°C in Middlebrook 7H9 medium supplemented with 10% oleic acid/albumin/dextrose/catalase supplement, 0.05% Tween-80 and Hygromycin B (50 µg/ml). *M. bovis* BCG Pasteur expressing GFP was cultured in Sauton medium containing kanamycin (25 µg/ml) and streptomycin (20 µg/ml). All mycobacterial cultures were maintained for up to 14 days before being used for the infection assay to reach the exponential phase of bacterial growth. Before infection, mycobacteria were washed three times with Dulbecco's phosphate-buffered saline (DPBS, Gibco) and resuspended in DPBS. For the assays performed with formalin-killed H37Rv, we incubated bacteria with 10% neutral buffered formalin (Sigma-Aldrich) for 1 h before washing them in DPBS.

4.4 | Mycobacterial infection and cell-based fluorescence assay

BMDCs (4×10^4 cells/well) and BMDMs (2×10^4 cells/well) were seeded in 384-well plates (Greiner) and infected with *Mycobacterium* sp. strains at an MOI of 1:1 in IMDM or RPMI medium supplemented with 10% heat-inactivated FCS for 2 h at 37°C (Deboosere et al., 2021). After two washes, the remaining extracellular bacilli in the infected cell suspension were killed by a 1-h treatment with amikacin (50 µg/ml, Sigma Aldrich). Cells were washed with the medium. Noninfected cells were also stimulated with LPS (100 ng/ml, InvivoGen) as a positive control for lipid droplet accumulation. Plates were incubated at 37°C and 5% CO₂ for 1 day up to 5 days.

At different time points, BMDCs were fixed with 10% neutral buffered formalin (Sigma-Aldrich) for 30 min, stained with 10 µg/ml Hoechst 33342 solution (Sigma) for 30 min, and washed twice with DPBS. Intracellular LDs were stained with a 2000-fold diluted HCS LipidTOX™ deep Red neutral lipid probe (Invitrogen) in DPBS for 30 min at RT. For kinetics of mycobacterial replication, cells were stained with 300 ng/ml Hoechst 33342 on the day of the infection, and image acquisition was performed daily for up to 3 days. All assays presented in this article were performed in the Biosafety Level 3 facility (BSL3).

4.5 | Image acquisition

Image acquisitions were performed using an automated confocal microscope Opera™ (PerkinElmer) equipped with 20X and 63X water objectives and with excitation lasers and cameras associated with a set of filters covering a detection wavelength ranging from 450 to 690 nm. Hoechst 33342-stained nuclei were detected using a 405-nm laser with a 450/50-nm emission filter. Green or red signals corresponding to BCG-GFP, H37Ra-GFP, H37Rv-GFP, or H37Rv-RFP were recorded using 488- or 561-nm lasers with 540/75- or 600/40-nm emission filters, respectively. The LipidTOX signal was detected using 630 nm excitation and 690 nm emission wavelengths. At least nine fields were recorded for each well, and each image

was processed and analyzed using the Columbus™ 2.7.0 system (PerkinElmer). Data are represented as the mean from one biological replicate of at least 4 replicated wells. Image segmentation was performed as indicated in Figures S1 and S2.

4.6 | General image analysis pipeline

At least three fields for each well were acquired. Images from 384-well plates were analyzed as described previously (Song et al., 2017). Briefly, to detect the intracellular bacteria and lipid droplets, each field was analyzed using the image-based analysis software Acapella 2.6 (Perkin Elmer). For each field, three channels were recorded: one for the green fluorescent bacteria (green), one for LipidTox/Lipid droplets (red), and one for the Hoechst/cell nuclei (blue channel). Three-color images were then segmented (Figure S1) using the following implementation procedures: (i) nuclei detection was performed using a built-in Acapella procedure; (ii) cytoplasm detection, based on the nuclei population, was performed using a built-in Acapella procedure; (iii) exclusion of cells on the edge of the image was performed using a built-in Acapella procedure; (iv) bacteria detection was performed by retaining only pixels whose intensities were higher than a manually defined threshold; (v) lipid droplet detection was performed by retaining only pixels whose intensities were higher than a manually defined threshold; and (vi) to identify infected cells, the positions of cells, and those of bacteria were merged (Figure S2). The results are expressed as the averages of the corresponding fields, including the total bacterial area, the total number of cells, the percentage of infected cells, and lipid droplets per cell (number, area, and/or mean of fluorescence intensity).

4.7 | CFU determination

At the indicated time points, cells were washed three times with DPBS and lysed with 0.1% sodium dodecyl sulfate (SDS) solution for bacterial counting. Serial dilutions (10^{-1} – 10^{-4}) were performed in DPBS, and 10 µl of each dilution was plated onto 7H11 agar plates supplemented with 10% OADC. *Mtb* colony numbers were determined, and the average of three plates of at least two dilutions was considered to determine the intracellular CFU per well. The average colony counts for each well were normalized to CFUs per ml.

4.8 | Quantitative PCR (qPCR)

RNA was extracted with QIAamp Viral RNA (Qiagen®) from cells seeded (10^5 cells/well) in 24-well plates, following the directions of the reagent. Quantitative RT-PCR was performed using a dye-based GoTaq® 1-Step RT-qPCR System (Promega, Fitchburg, WI, USA) in a StepOne™ Real-Time PCR System (Thermo Fisher, Carlsbad, CA,

USA). Amplifications were carried out in 15 μ l reaction mixtures containing 2 \times reaction mix buffer, 1 \times of probe-based oligos from pre-designed TaqMan Gene Expression Assays (Thermo Fisher, Carlsbad, CA, USA), and 5 μ l of RNA template. The program for probe-based amplifications was 10 min at 95°C followed by 50 cycles of 15 s at 95°C and 1 min at 60°C. The relative mRNA expression was calculated by the 2^{- $\Delta\Delta$ Ct} method. β -actin (*actb*) expression was used as a reference gene. The probe-based oligos were all Pre-designed Taqman Gene Expression Assays: *il-1 β* (ref: Mm00434228_m1, FAM), *il-10* (ref: Mm00439614_m1, FAM), *cox-2/ptgs2* (ref: Mm00478374_m1, FAM), *5-lo/alo5* (ref: Mm01182747_m1, FAM), *inos/nos2* (ref: Mm00440502_m1, FAM), *arg1* (ref: Mm00475988_m1, FAM), *chi3l3/ym1* (ref: Mm00657889_m1, FAM), *mr1* (ref: Mm00468487_m1, FAM), *fasn* (ref: Mm00662322_g1, FAM), *dgat1* (ref: Mm00515643_m1, FAM), *dgat2* (ref: Mm00499536_m1, FAM), *acat1* (ref: Mm00507463_m1, FAM), *plin2* (ref: Mm00475794_m1, FAM), *plin3* (ref: Mm04208646_g1), *atgl/pnpla2* (ref: Mm00503040_m1, FAM), *cd36* (ref: Mm01135198_m1, FAM), β -actin/*actb* (ref: Mm02619580_g1, FAM).

4.9 | Thin-layer chromatography (TLC)

The lipid fractions from 10⁵ DMDCs were extracted by applying the Bligh and Dyer (1959). TLC was performed on silica gel 60 plates (Merck) according to Horwitz and Perlman (1987) (Horwitz & Perlman, 1987). Plates were developed in hexane/ethyl ether/acetic acid solution (60:40:1, v/v) until the solvent front reached the upper line. Neutral lipids were identified by comparison with standard lipids (1 mg/ml): cholesterol (CHO), cholesterol ester (CE), fatty acid (FA), monoacylglycerol (MAG), diacylglycerol (DAG), and triacylglycerol (TAG), obtained from Sigma. For visualization of lipids, the TLC plates were stained by spraying with Charring reagent (3% CuSO₄ and 8% H₃PO₄ v/v) and heating at 110°C for 10 min.

4.10 | Statistical analysis

Data from one representative experiment of three independent experiments are reported as the mean \pm SEM and were analyzed statistically using analysis of variance (ANOVA) followed by Student's *t*-test. Values of *p* \leq 0.05 were regarded as significant.

AUTHOR CONTRIBUTIONS

Maria Fernanda de Souza Costa: Conceptualization; data curation; formal analysis; investigation; methodology; writing – original draft; writing – review and editing. **Filipe Santos Pereira-Dutra:** Conceptualization; formal analysis; methodology; writing – review and editing. **Nathalie Deboosere:** Formal analysis; investigation; methodology; writing – review and editing. **Samuel Jouny:** Methodology. **Ok-Ryul Song:** Formal analysis; methodology; writing – review and editing. **Guilherme Iack:** Methodology.

Andrea Lamoglia Souza: Methodology. **Ric Henrique Roma:** Methodology; resources. **Vincent Delorme:** Formal analysis; methodology; writing – review and editing. **Patricia T. Bozza:** Resources; writing – review and editing. **Priscille M. Brodin:** Conceptualization; funding acquisition; resources; supervision; writing – review and editing.

ACKNOWLEDGMENTS

The authors are grateful to Dr. François Trottein (Institut Pasteur de Lille), who kindly provided the J558 cell line. This study was financed by the European Union (ERC-STG INTRACELLTB 260901, MM4TB 260872, and CycloNHit 608407), the ANR (ANR-10-EQPX-04-01, ANR-16-CE35-0009, and ANR-18-JAM2-0002), the Institut Pasteur (PTR441 and PTR430), the Feder (12001407 (D-AL) Equipex Imaginex BioMed), and the Région Nord Pas de Calais (12000080). MFS Costa was the recipient of a fellowship from Conselho Nacional de Desenvolvimento Científico e Tecnológico (CNPq). The funders had no role in the study design, data collection, analysis, decision to publish, or preparation of the manuscript.

CONFLICT OF INTEREST

The authors declare no competing interests.


DATA AVAILABILITY STATEMENT

The data that support this study findings of are available upon reasonable request to the corresponding author.

ETHICS STATEMENT

All experimental procedures using animals received ethical approval from the French Committee on Animal Experimentation and the Ministry of Education and Research (APAFIS#10232-2017061411305485 v6, approved on September 14, 2018).

ORCID

Maria Fernanda de Souza Costa  <https://orcid.org/0000-0003-2300-5384>

Filipe Pereira-Dutra  <https://orcid.org/0000-0003-1917-2876>

Vincent Delorme  <https://orcid.org/0000-0001-5235-7069>

REFERENCES

- Almeida, P.E., Silva, A.R., Maya-Monteiro, C.M., Töröcsik, D., D'Ávila, H., Dezsö, B. et al. (2009) *Mycobacterium bovis* Bacillus Calmette-Guérin infection induces TLR2-dependent peroxisome proliferator-activated receptor γ expression and activation: functions in inflammation, lipid metabolism, and pathogenesis. *The Journal of Immunology*, 183, 1337 – 1345.
- Barisch, C. & Soldati, T. (2017) *Mycobacterium marinum* degrades both Triacylglycerols and phospholipids from its dictyostelium host to synthesise its own triacylglycerols and generate lipid inclusions. *PLoS Pathogens*, 13, e1006095.
- Barisch, C., Paschke, P., Hagedorn, M., Maniak, M. & Soldati, T. (2015) Lipid droplet dynamics at early stages of *Mycobacterium marinum* infection in Dictyostelium. *Cellular Microbiology*, 17, 1332–1349.
- Bligh, E.G. & Dyer, W.J. (1959) A rapid method of total lipid extraction and purification. *Canadian Journal of Biochemistry and Physiology*, 37, 1475–1491.

- Bosch, M., Sánchez-Álvarez, M., Fajardo, A., Kapetanovic, R., Steiner, B., Dutra, F. et al. (2020) Mammalian lipid droplets are innate immune hubs integrating cell metabolism and host defense. *Science*, 1979, 370.
- Bougnères, L., Helfft, J., Tiwari, S., Vargas, P., Chang, B.H.J., Chan, L. et al. (2009) A role for lipid bodies in the cross-presentation of phagocytosed antigens by MHC class I in dendritic cells. *Immunity*, 31, 232–244.
- Brandenburg, J., Marwitz, S., Tazoll, S.C., Waldow, F., Kalsdorf, B., Vierbuchen, T. et al. (2021) WNT6/ACC2-induced storage of triacylglycerols in macrophages is exploited by *Mycobacterium tuberculosis*. *Journal of Clinical Investigation*, 131, e141833.
- Brzostek, A., Pawelczyk, J., Rumijowska-Galewicz, A., Dziadek, B. & Dziadek, J. (2009) *Mycobacterium tuberculosis* is able to accumulate and utilize cholesterol. *Journal of Bacteriology*, 191, 6584–6591.
- Buettner, M., Meinken, C., Bastian, M., Bhat, R., Stössel, E., Faller, G. et al. (2005) Inverse correlation of maturity and antibacterial activity in human dendritic cells. *The Journal of Immunology*, 174, 4203–4209.
- Caire-Brändli, I.B., Papadopoulos, A., Malaga, W., Marais, D., Canaan, S., Thilo, L. et al. (2014) Reversible lipid accumulation and associated division arrest of *Mycobacterium avium* in lipoprotein-induced foamy macrophages may resemble key events during latency and reactivation of tuberculosis. *Infection and Immunity*, 82, 476–490.
- Christophe, T., Jackson, M., Hee, K.J., Fenistein, D., Contreras-Dominguez, M., Kim, J. et al. (2009) High content screening identifies decaprenyl-phosphoribose 2' epimerase as a target for intracellular antimycobacterial inhibitors. *PLoS Pathogens*, 5, e1000645.
- Clemens, D.L. & Horwitz, M.A. (1995) Characterization of the *Mycobacterium tuberculosis* phagosome and evidence that phagosomal maturation is inhibited. *Journal of Experimental Medicine*, 181, 257–270.
- Daniel, J., Maamar, H., Deb, C., Sirakova, T.D. & Kolattukudy, P.E. (2011) *Mycobacterium tuberculosis* uses host triacylglycerol to accumulate lipid droplets and acquires a dormancy-like phenotype in lipid-loaded macrophages. *PLoS Pathogens*, 7, e1002093.
- Dartois, V.A. & Rubin, E.J. (2022) Anti-tuberculosis treatment strategies and drug development: challenges and priorities. *Nature Reviews. Microbiology*, 20, 685–701.
- D'Avila, H., Melo, R.C.N., Parreira, G.G., Werneck-Barroso, E., Castro-Faria-Neto, H.C. & Bozza, P.T. (2006) *Mycobacterium bovis* Bacillus Calmette-Guérin induces TLR2-mediated formation of lipid bodies: intracellular domains for eicosanoid synthesis *In vivo*. *The Journal of Immunology*, 176, 3087–3097.
- Dawa, S., Menon, D., Arumugam, P., Bhaskar, A.K., Mondal, M., Rao, V. et al. (2021) Inhibition of granuloma triglyceride synthesis imparts control of *Mycobacterium tuberculosis* through curtailed inflammatory responses. *Frontiers in Immunology*, 12, 722735.
- Deboosere, N., Belhaouane, I., Machelart, A., Hoffmann, E., Vandeputte, A. & Brodin, P. (2021) High-content analysis monitoring intracellular trafficking and replication of *Mycobacterium tuberculosis* inside host cells. *Methods in Molecular Biology*, 2314, 649–702.
- Etna, M.P., Giacomini, E., Pardini, M., Severa, M., Bottai, D., Cruciani, M. et al. (2015) Impact of *Mycobacterium tuberculosis* RD1-locus on human primary dendritic cell immune functions. *Scientific Reports*, 5, 17078.
- Förtsch, D., Rölinghoff, M. & Stenger, S. (2000) IL-10 converts human dendritic cells into macrophage-like cells with increased antibacterial activity against virulent *Mycobacterium tuberculosis*. *The Journal of Immunology*, 165, 978–987.
- Gao, F., Liu, C., Guo, J., Sun, W., Xian, L., Bai, D. et al. (2015) Radiation-driven lipid accumulation and dendritic cell dysfunction in cancer. *Scientific Reports*, 5, 9613. Available from: <http://www.nature.com/articles/srep09613>
- Herber, D.L., Cao, W., Nefedova, Y., Novitskiy, S.v., Nagaraj, S., Tyurin, V.A. et al. (2010) Lipid accumulation and dendritic cell dysfunction in cancer. *Nature Medicine*, 16, 880–886.
- Horwitz, J. & Perlman, R.L. (1987) Measurement of inositol phospholipid metabolism in PC12 Pheochromocytoma cells. *Methods in Enzymology*, 141, 169–175.
- Hunter, R.L., Welsh, K.J., Risin, S.A. & Actor, J.K. (2011) Immunopathology of postprimary tuberculosis: increased T-regulatory cells and DEC-205-positive foamy macrophages in cavitory lesions. *Clinical & Developmental Immunology*, 2011, 307631.
- Jia, X., Yang, L., Dong, M., Chen, S., Lv, L., Cao, D. et al. (2017) The bioinformatics analysis of comparative genomics of *Mycobacterium tuberculosis* complex (MTBC) provides insight into dissimilarities between intraspecific groups differing in host association, virulence, and epitope diversity. *Frontiers in Cellular and Infection Microbiology*, 7, 88.
- Kapoor, N., Pawar, S., Sirakova, T.D., Deb, C., Warren, W.L. & Kolattukudy, P.E. (2013) Human granuloma *In vitro* model, for TB dormancy and resuscitation. *PLoS One*, 8, e53657.
- Kelly, B. & O'Neill, L.A.J. (2015) Metabolic reprogramming in macrophages and dendritic cells in innate immunity. *Cell Research*, 25, 771–784.
- Kilinc, G., Saris, A., Ottenhoff, T.H.M. & Haks, M.C. (2021) Host-directed therapy to combat mycobacterial infections*. *Immunological Reviews*, 301, 62–83.
- Kim, W.S., Kim, J.S., Cha, S., bin, Kim, H., Kwon, K.W., Kim, S.J. et al. (2016) *Mycobacterium tuberculosis* Rv3628 drives th1-type T cell immunity via TLR2-mediated activation of dendritic cells and displays vaccine potential against the hyper-virulent Beijing K strain. *Oncotarget*, 7, 24962–24982.
- Knight, M., Braverman, J., Asfaha, K., Gronert, K. & Stanley, S. (2018) Lipid droplet formation in *Mycobacterium tuberculosis* infected macrophages requires IFN- γ /HIF-1 α signaling and supports host defense. *PLoS Pathogens*, 14, e1006874.
- Laval, T., Chaumont, L. & Demangel, C. (2021) Not too fat to fight: the emerging role of macrophage fatty acid metabolism in immunity to *Mycobacterium tuberculosis*. *Immunological Reviews*, 301, 84–97.
- Lecoeur, H., Giraud, E., Prévost, M.C., Milon, G. & Lang, T. (2013) Reprogramming neutral lipid metabolism in mouse dendritic leukocytes hosting live *Leishmania amazonensis* amastigotes. *PLoS Neglected Tropical Diseases*, 7, e2276.
- Machelart, A., Belhaouane, I., Deboosere, N., Poncin, I., Saint-André, J.-P., Pauwels, A.-M. et al. (2022) IRG1 controls host responses to restrict *Mycobacterium tuberculosis* infection. *bioRxiv*. <https://www.biorxiv.org/content/10.1101/761551v2.full>
- Mahajan, S., Dkhar, H.K., Chandra, V., Dave, S., Nanduri, R., Janmeja, A.K. et al. (2012) *Mycobacterium tuberculosis* modulates macrophage lipid-sensing nuclear receptors PPAR γ and TR4 for survival. *The Journal of Immunology*, 188, 5593–5603.
- Majlessi, L., Brodin, P., Brosch, R., Rojas, M.-J., Khun, H., Huerre, M. et al. (2005) Influence of ESAT-6 secretion system 1 (RD1) of *Mycobacterium tuberculosis* on the interaction between mycobacteria and the host immune system. *The Journal of Immunology*, 174, 3570–3579.
- Mattos, K.A., Oliveira, V.G.C., D'Avila, H., Rodrigues, L.S., Pinheiro, R.O., Sarno, E.N. et al. (2011) TLR6-driven lipid droplets in *Mycobacterium leprae*-infected Schwann cells: Immunoinflammatory platforms associated with bacterial persistence. *The Journal of Immunology*, 187, 2548–2558.
- Meester, I., Rosas-Taraco, A.G. & Salinas-Carmona, M.C. (2014) *Nocardia brasiliensis* induces formation of foamy macrophages and dendritic cells *in vitro* and *in vivo*. *PLoS One*, 9, e100064.
- Mendum, T.A., Wu, H., Kierzek, A.M. & Stewart, G.R. (2015) Lipid metabolism and type VII secretion systems dominate the genome scale virulence profile of *Mycobacterium tuberculosis* in human dendritic cells. *BMC Genomics*, 16, 372.
- Morris, D., Gonzalez, B., Khurasany, M., Kassissa, C., Luong, J., Kasko, S. et al. (2013) Characterization of dendritic cell and regulatory T cell functions against *Mycobacterium tuberculosis* infection. *BioMed Research International*, 2013, 402827.

- Mostowy, S., Cousins, D. & Behr, M.A. (2004) Genomic interrogation of the Dassie bacillus reveals it as a unique RD1 mutant within the *Mycobacterium tuberculosis* complex. *Journal of Bacteriology*, *186*, 104–109.
- Muñoz-Eliás, E.J. & McKinney, J.D. (2005) *Mycobacterium tuberculosis* isocitrate lyases 1 and 2 are jointly required for *in vivo* growth and virulence. *Nature Medicine*, *11*, 638–644.
- Neyrolles, O. (2014) Mycobacteria and the greasy macrophage: getting fat and frustrated. *Infection and Immunity*, *82*, 472–475.
- Olakanmi, O., Kesavalu, B., Abdalla, M.Y. & Britigan, B.E. (2013) Iron acquisition by *Mycobacterium tuberculosis* residing within myeloid dendritic cells. *Microbial Pathogenesis*, *65*, 21–28.
- O'Neill, L.A.J. & Pearce, E.J. (2016) Immunometabolism governs dendritic cell and macrophage function. *Journal of Experimental Medicine*, *213*, 15–23.
- Ordway, D., Henao-Tamayo, M., Orme, I.M. & Gonzalez-Juarrero, M. (2005) Foamy macrophages within lung granulomas of mice infected with *Mycobacterium tuberculosis* express molecules characteristic of dendritic cells and Antiapoptotic markers of the TNF receptor-associated factor family. *The Journal of Immunology*, *175*, 3873–3881.
- Pandey, A.K. & Sasseti, C.M. (2008) Mycobacterial persistence requires the utilization of host cholesterol. *Proceedings of the National Academy of Sciences of the United States of America*, *105*, 4376–4380.
- Pereira-Dutra, F.S., Teixeira, L., de Souza Costa, M.F. & Bozza, P.T. (2019) Fat, fight, and beyond: the multiple roles of lipid droplets in infections and inflammation. *Journal of Leukocyte Biology*, *106*(3), 563–580.
- Peyron, P., Vaubourgeix, J., Poquet, Y., Levillain, F., Botanch, C., Bardou, F. et al. (2008) Foamy macrophages from tuberculous patients' granulomas constitute a nutrient-rich reservoir for *M. tuberculosis* persistence. *PLoS Pathogens*, *4*, e1000204.
- Pym, A.S., Brodin, P., Brosch, R., Huerre, M. & Cole, S.T. (2002) Loss of RD1 contributed to the attenuation of the live tuberculosis vaccines *Mycobacterium bovis* BCG and *Mycobacterium microti*. *Molecular Microbiology*, *46*, 709–717.
- Rivero-Lezcano, O.M., González-Cortés, C., Reyes-Ruvalcaba, D. & Diez-Tascón, C. (2010) CCL20 is overexpressed in *Mycobacterium tuberculosis*-infected monocytes and inhibits the production of reactive oxygen species (ROS). *Clinical and Experimental Immunology*, *162*, 289–297.
- Rodrigues, T.S., Conti, B.J., Fraga-Silva, T.F.d.C., Almeida, F. & Bonato, V.L.D. (2020) Interplay between alveolar epithelial and dendritic cells and *Mycobacterium tuberculosis*. *Journal of Leukocyte Biology*, *108*, 1139–1156.
- Roque, N.R., Lage, S.L., Navarro, R., Fazolini, N., Maya-Monteiro, C.M., Rietdorf, J. et al. (2020) Rab7 controls lipid droplet-phagosome association during mycobacterial infection. *Biochimica et Biophysica Acta - Molecular and Cell Biology of Lipids*, *1865*, 158703.
- Salvatore, G., Bernoud-Hubac, N., Bissay, N., Debard, C., Daira, P., Meugnier, E. et al. (2015) Human monocyte-derived dendritic cells turn into foamy dendritic cells with IL-17A. *Journal of Lipid Research*, *56*, 1110–1122.
- Santucci, P., Bouzid, F., Smichi, N., Poncin, I., Kremer, L., de Chastellier, C. et al. (2016) Experimental models of foamy macrophages and approaches for dissecting the mechanisms of lipid accumulation and consumption during dormancy and reactivation of tuberculosis. *Frontiers in Cellular and Infection Microbiology*, *6*, 122.
- Schreiber, H.A., Harding, J.S., Hunt, O., Altamirano, C.J., Hulseberg, P.D., Stewart, D. et al. (2011) Inflammatory dendritic cells migrate in and out of transplanted chronic mycobacterial granulomas in mice. *Journal of Clinical Investigation*, *121*, 3902–3913.
- Simeone, R., Bottai, D., Frigui, W., Majlessi, L. & Brosch, R. (2015) ESX/ type VII secretion systems of mycobacteria: insights into evolution, pathogenicity and protection. *Tuberculosis*, *95*, S150–S154.
- Singh, V., Jamwal, S., Jain, R., Verma, P., Gokhale, R. & Rao, K.V.S. (2012) *Mycobacterium tuberculosis*-driven targeted recalibration of macrophage lipid homeostasis promotes the foamy phenotype. *Cell Host & Microbe*, *12*, 669–681.
- Song, O.R., Deboosere, N., Delorme, V., Queval, C.J., Deloison, G., Werkmeister, E. et al. (2017) Phenotypic assays for *Mycobacterium tuberculosis* infection. *Cytometry Part A*, *91*, 983–994.
- Srivastava, S., Ernst, J.D. & Desvignes, L. (2014) Beyond macrophages: the diversity of mononuclear cells in tuberculosis. *Immunological Reviews*, *262*, 179–192.
- Tailleux, L., Neyrolles, O., Honoré-Bouakline, S., Perret, E., Sanchez, F., Abastado, J.-P., Lagrange, P. H., Gluckman, J. C., Rosenzweig, M., & Herrmann, J.-L. (2003) Constrained Intracellular Survival of *Mycobacterium tuberculosis* in Human Dendritic Cells. *The Journal of Immunology*, *170*, 1939–1948.
- Tian, T., Woodworth, J., Sköld, M. & Behar, S.M. (2005) *In vivo* depletion of CD11c + cells delays the CD4 + T cell response to *Mycobacterium tuberculosis* and exacerbates the outcome of infection. *The Journal of Immunology*, *175*, 3268–3272.
- Tzelepis, F., Verway, M., Daoud, J., Gillard, J., Hassani-Ardakani, K., Dunn, J. et al. (2015) Annexin1 regulates DC efferocytosis and cross-presentation during *Mycobacterium tuberculosis* infection. *Journal of Clinical Investigation*, *125*, 752–768.
- Uehira, K., Amakawa, R., Ito, T., Tajima, K., Naitoh, S., Ozaki, Y. et al. (2002) Dendritic cells are decreased in blood and accumulated in granuloma in tuberculosis. *Clinical Immunology*, *105*, 296–303.
- Wolf, A.J., Linas, B., Trevejo-Nuñez, G.J., Kincaid, E., Tamura, T., Takatsu, K. et al. (2007) *Mycobacterium tuberculosis* infects dendritic cells with high frequency and impairs their function *In vivo*. *The Journal of Immunology*, *179*, 2509 – 2519.
- World Health Organization. (2022) *Global tuberculosis report 2022*. Geneva: World Health Organization.
- Zhang, X., Li, S., Luo, Y., Chen, Y., Cheng, S., Zhang, G. et al. (2013) *Mycobacterium bovis* and BCG induce different patterns of cytokine and chemokine production in dendritic cells and differentiation patterns in CD4+T cells. *Microbiology (United Kingdom)*, *159*, 366–379.

SUPPORTING INFORMATION

Additional supporting information can be found online in the Supporting Information section at the end of this article.

How to cite this article: Costa, M. F. d. S., Pereira-Dutra, F., Deboosere, N., Jouny, S., Song, O.-R., lack, G., Souza, A. L., Roma, E. H., Delorme, V., Bozza, P. T. & Brodin, P. (2023). *Mycobacterium tuberculosis* induces delayed lipid droplet accumulation in dendritic cells depending on bacterial viability and virulence. *Molecular Microbiology*, *119*, 224–236. <https://doi.org/10.1111/mmi.15023>